Supporting Information

Molybdenum Carbide-Embedded Nitrogen-Doped Porous Carbon Nanosheets as Electrocatalysts for Water Splitting in Alkaline Media

Chenbao Lu[†,‡], *Diana Tranca*[§], *Jian Zhang*[§], *Fermín Rodríguez-Hernández*[§,∥,⊥], *Yuezeng Su*[‡], *Xiaodong Zhuang**[,†], *Fan Zhang**[,†], *Gotthard Seifert*[§], *Xinliang Feng**[,†,§]

[†]School of Chemistry and Chemical Engineering, State Key Laboratory of Metal Matrix Composites, Shanghai Key Laboratory of Electrical Insulation and Thermal Ageing, Shanghai Jiao Tong University, 200240 Shanghai, P. R. China.
E-mail: zhuang@sjtu.edu.cn, fan-zhang@sjtu.edu.cn,
[‡]School of Electronic Information and Electrical Engineering, School of Aeronautics and Astronautics, Shanghai Jiao Tong University, 200240 Shanghai, P. R. China.
[§]Center for Advancing Electronics Dresden (cfaed) & Department of Chemistry and Food Chemistry, Technische Universität Dresden, Mommsenstrasse 4, 01062 Dresden, Germany.
E-mail: xinliang.feng@tu-dresden.de
[∥]Theoretical Chemistry, Technische Universität Dresden, Mommsenstr. 13, Dresden 01062, Germany.
[⊥]DynAMoS (Dynamical processes in Atomic and Molecular Systems), Facultad de Física, Universidad de La Habana, San Lázaro y L, La Habana 10400, Cuba.

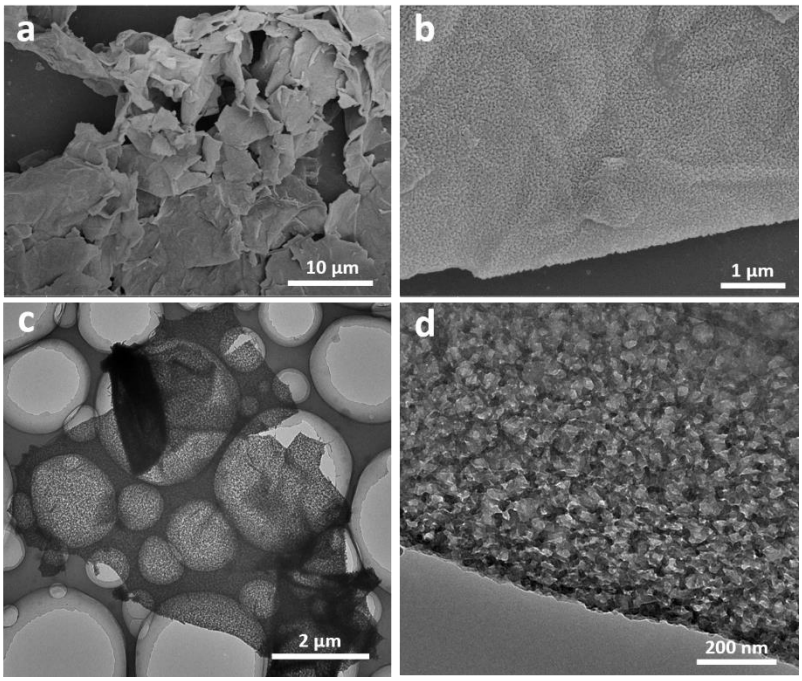

Figure S1. (a, b) SEM, (c, d) TEM images of Mo@2D-PANI; Many uniform nanosheets can be observed and no naked graphene nanosheets or free polyaniline nanofibers were observed, which indicates that most of the aniline monomers have been polymerized on the surface of graphene.

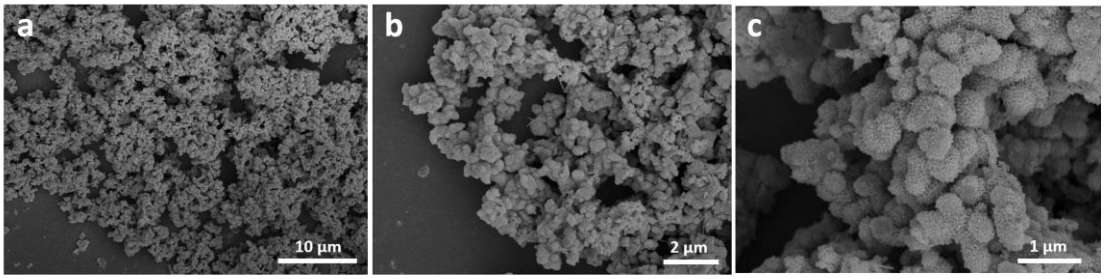

Figure S2. (a, b, and c) SEM images of Mo@PANI; the results indicate that the PANI tend to aggregation without GO.

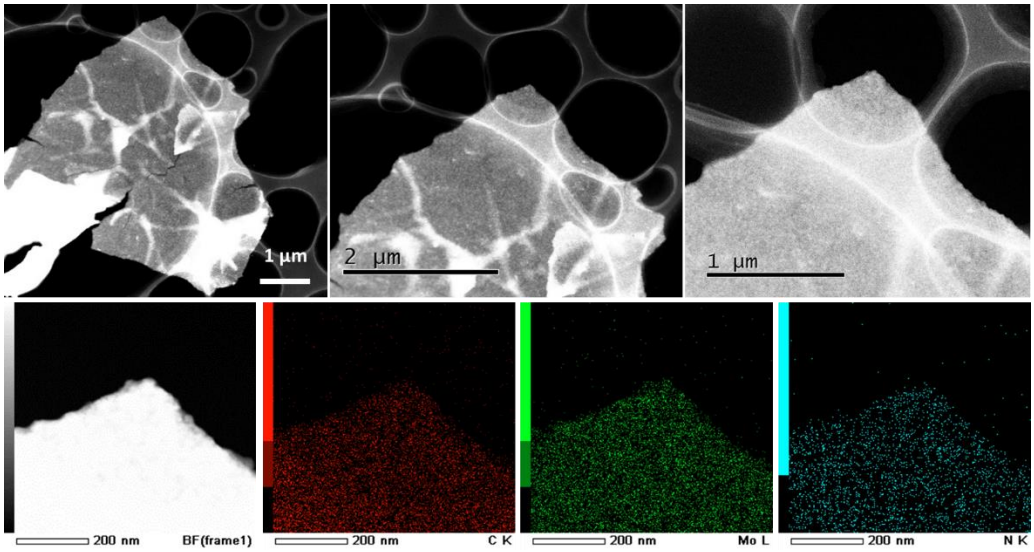

Figure S3. HAADF-STEM images and elemental mapping for Mo@2D-PANI, reveal the uniform distribution of Mo in the PANI nanosheets.

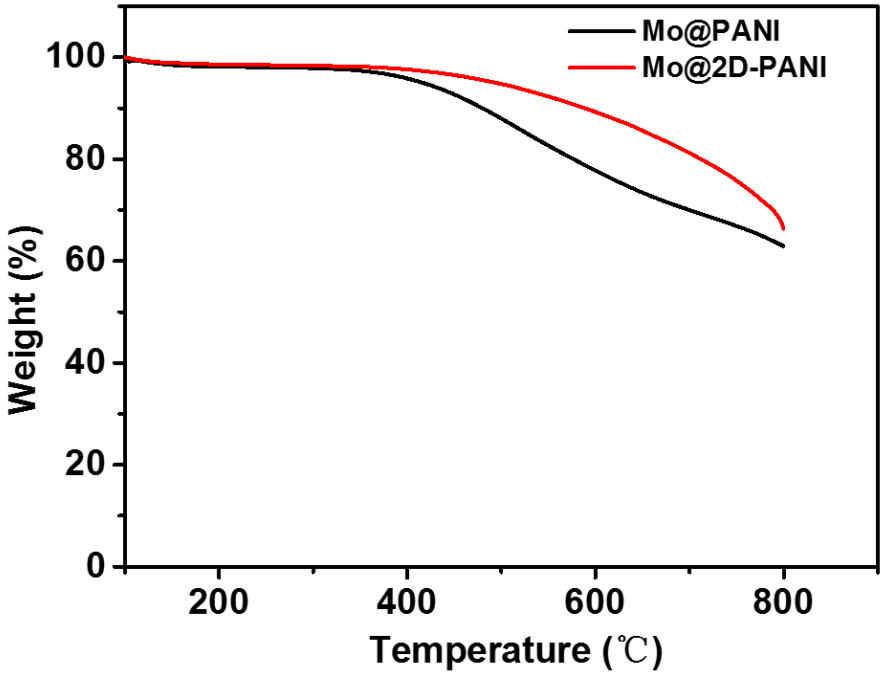

Figure S4. TGA curve of the as-prepared Mo@PANI and Mo@2D-PANI from 100 to 800 ℃ under N_2 gas flow with a temperature ramp of 5 ℃ min^{-1}.The thermal property of these hybrids show that the decomposition reaction mainly occur at about 400 ℃, and the remaining weight of samples after heating to 800 ℃ are about 65%.

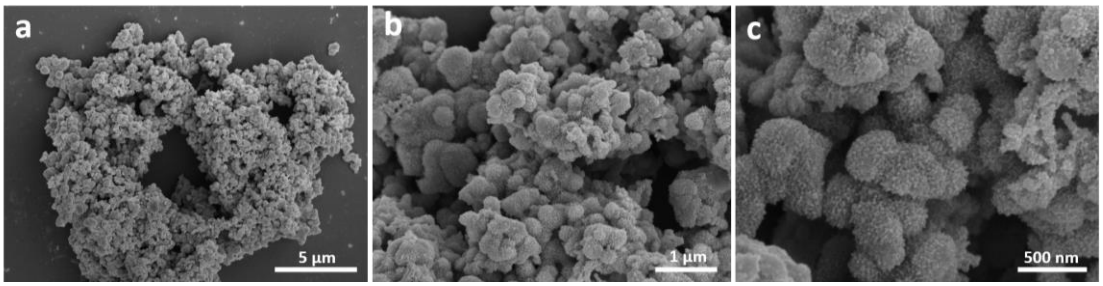

Figure S5. (a, b, and c) SEM images of Mo_2C@NPC.

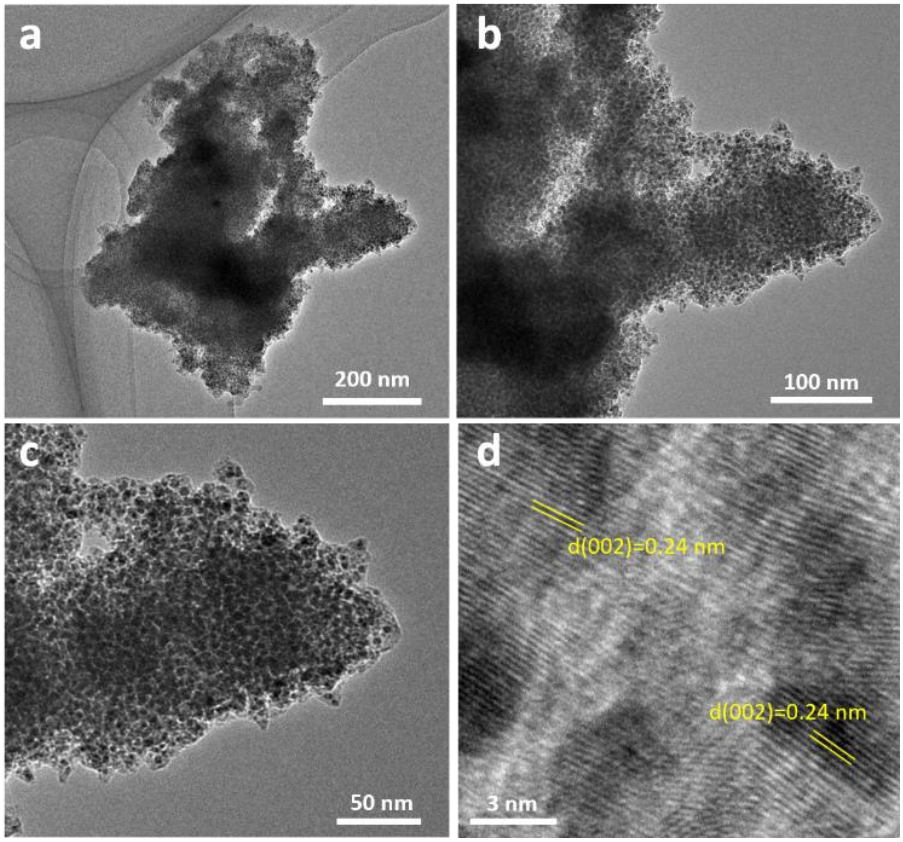

Figure S6. TEM images of Mo_2C@NPC. HR-TEM image (d) shows clear lattice fringe with interplanar distance of 0.24 nm, which correspond to the (002) crystal planes of Mo_2C nanoparticles. Figure S5 and S6 reveal that PANI tend to aggregation without GO, and then it tends to form large Mo_2C nanoparticles after carbonized, which decrease the exposed active surface. Notably, using GO as the templates can effectively prevent the aggregation and overlapping growth of Mo_2C nanoparticles.

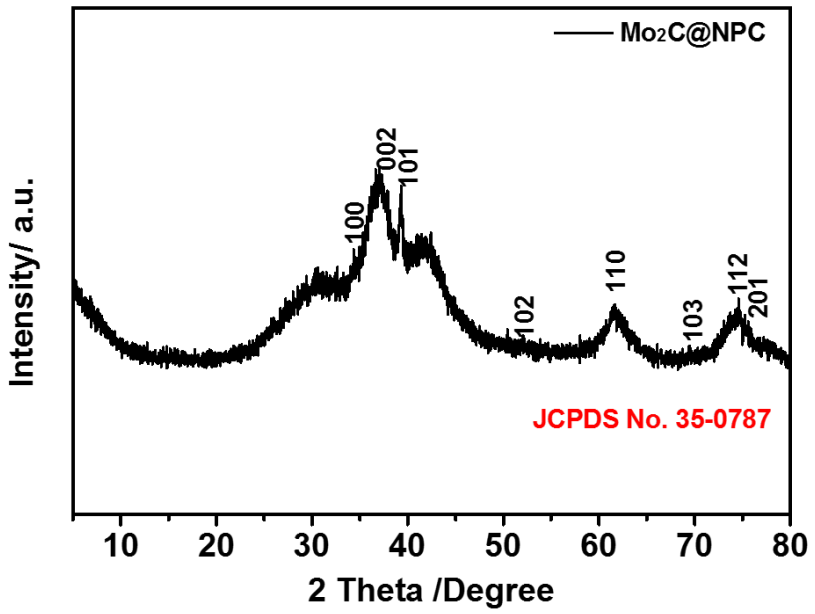

Figure S7. XRD patterns of Mo_2C@NPC. All XRD peaks can be indexed to crystalline Mo_2C (JCPDS No. 35-0787).

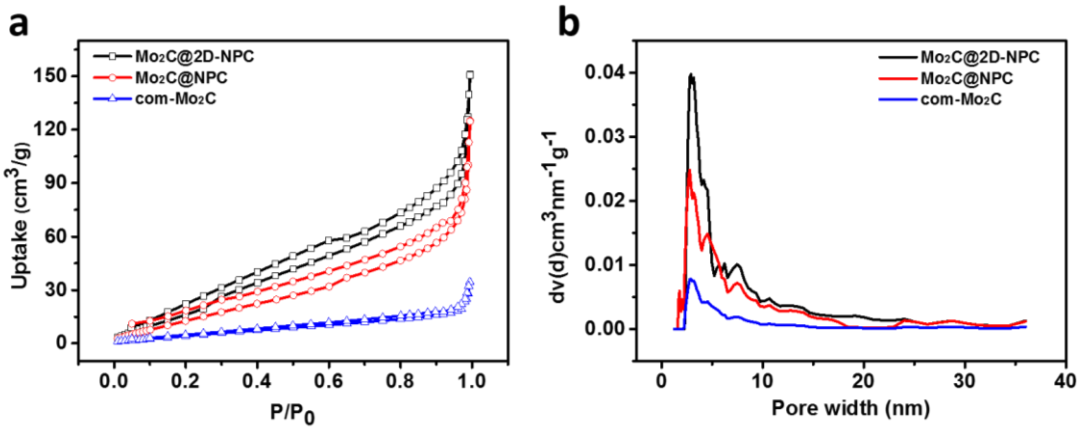

Figure S8. (a) N_2 sorption isotherms of Mo_2C@2D-NPC, Mo_2C@NPC, and com-Mo_2C; (b) the pore size distribution calculated from NLDFT method. The pore diameter mainly centered between 2-10 nm.

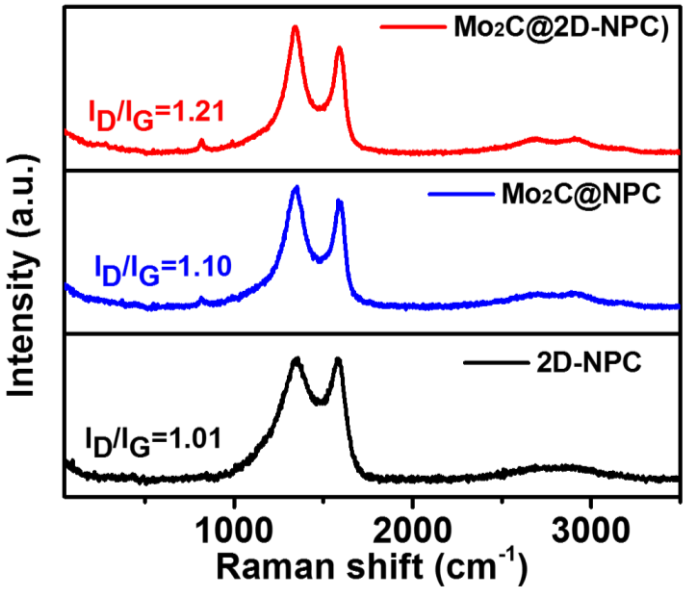

Figure S9. Raman spectra of Mo_2C@2D-NPC (red), Mo_2C@NPC (blue), and 2D-NPC (black). The I_D/I_G of Mo_2C@2D-NPC is 1.21, which is higher than that of 2D-NPC (1.01) and Mo_2C@NPC (1.10), suggesting more active defects in Mo_2C@2D-NPC.

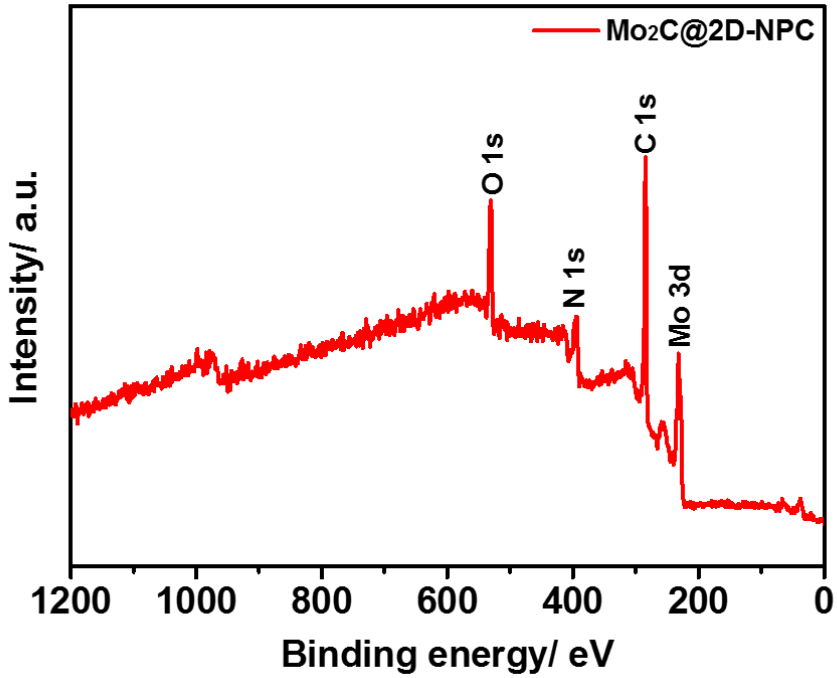

Figure S10. XPS spectrum of Mo_2C@2D-NPC, demonstrates the existence of C, Mo, N and O elements.

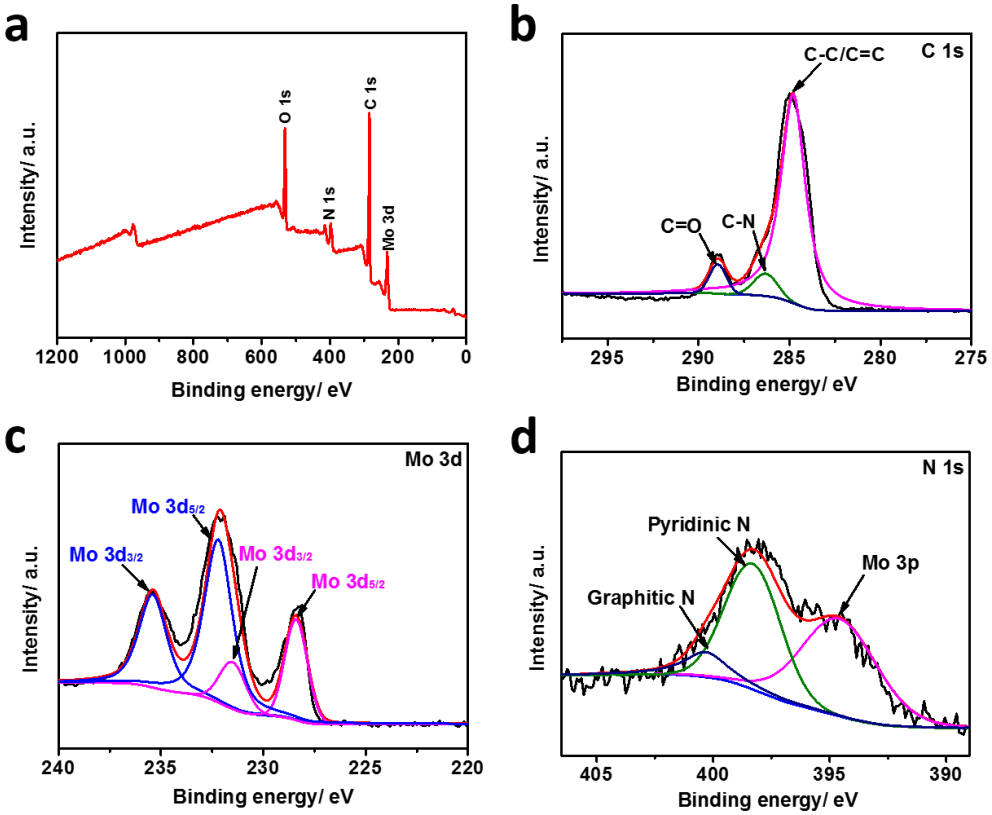

Figure S11. XPS spectrum of (a) Mo_2C@NPC. High-resolution XPS spectra of (b) C 1s, (c) Mo 3d, (d) N 1s of Mo_2C@NPC.

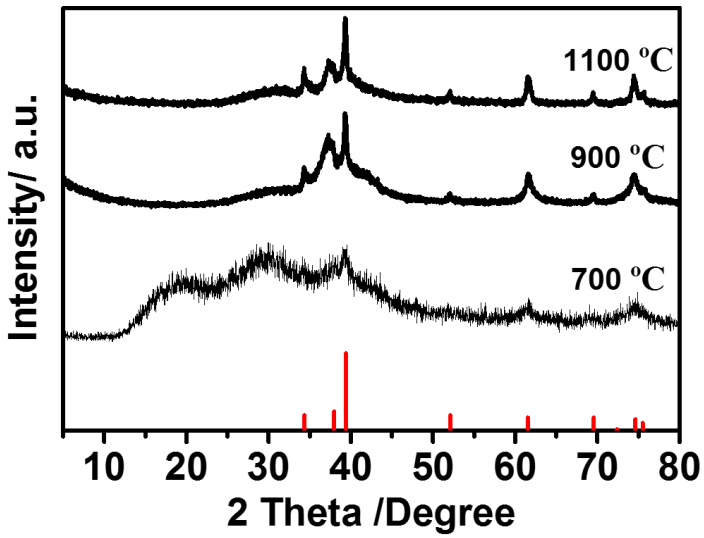

Figure S12. XRD patterns of Mo_2C@2D-NPC/700, Mo_2C@2D-NPC, and Mo_2C@2D-NPC/1100. All XRD peaks can be indexed to crystalline Mo_2C (JCPDS No. 35-0787). The results reveal that when carbonization under 700 ℃, it shows poor crystalline structure.

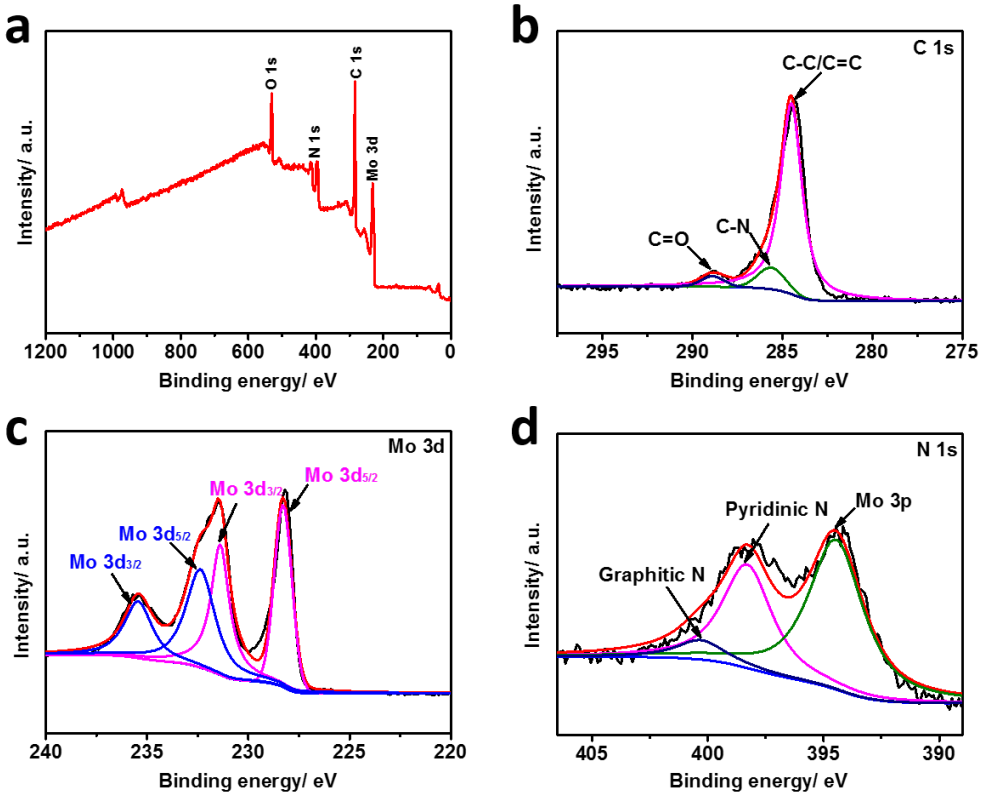

Figure S13. XPS spectrum of (a) Mo_2C@2D-NPC/700. High-resolution XPS spectra of (b) C 1s, (c) Mo 3d, (d) N 1s of Mo_2C@2D-NPC/700.

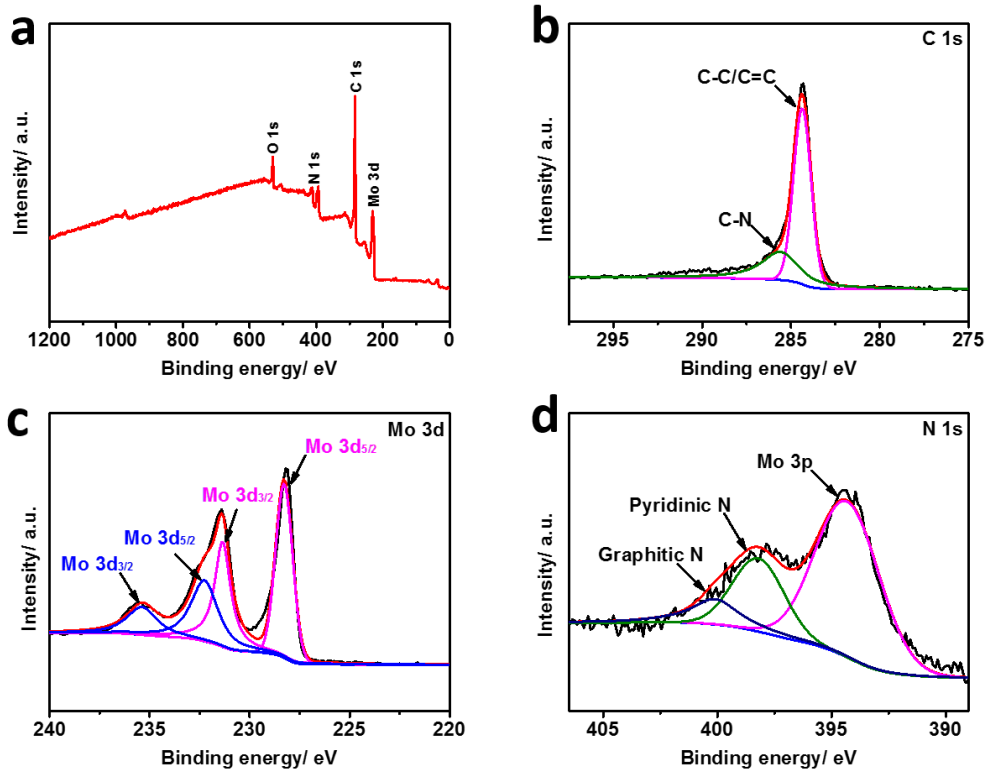

Figure S14. XPS spectrum of (a) Mo_2C@2D-NPC/1100. High-resolution XPS spectra of (b) C 1s, (c) Mo 3d, (d) N 1s of Mo_2C@2D-NPC/1100.

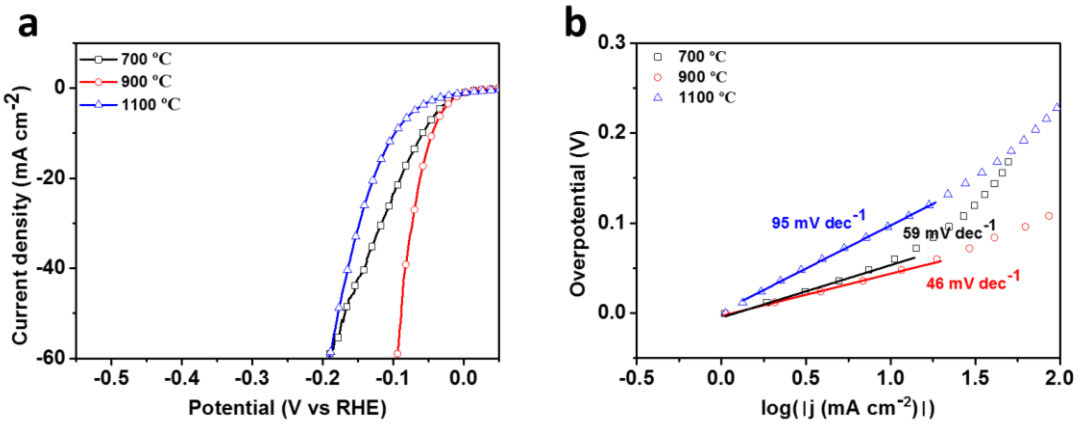

Figure S15. HER performance of Mo_2C@2D-NPC at different carbonization temperature in basic media. (a) Polarization curves and (b) corresponding Tafel plots of as-prepared materials in 1M KOH. This result indicate that the catalyst carbonized at 900 ℃ exhibited the best HER performance.

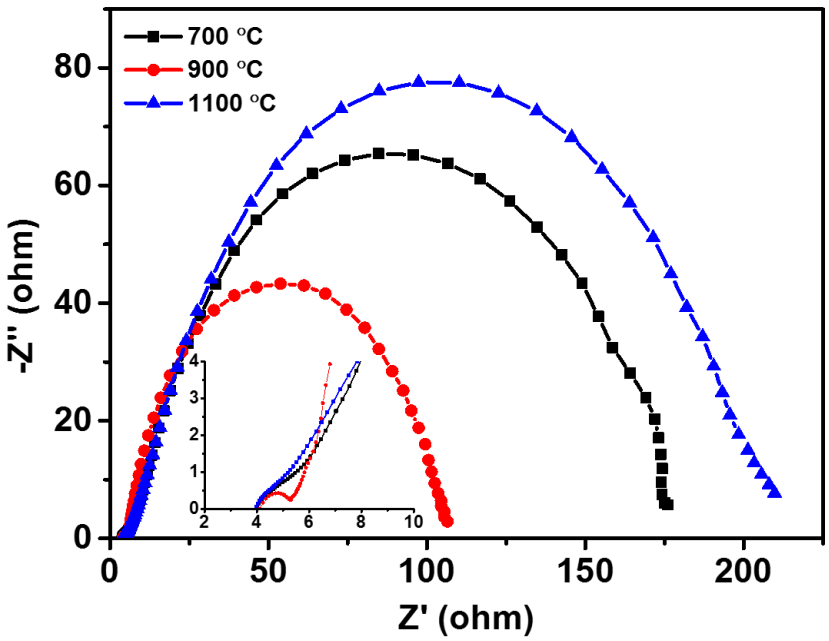

Figure S16. Nyquist plots of Mo_2C@2D-NPC at different carbonization temperature over the frequency range from 1000 kHz to 0.02 Hz at the open-circuit voltage with an AC voltage of 10 mV. Inset: the enlarged Nyquist plots in high frequency zone. Compared with the Nyquist plot of Mo_2C@2D-NPC/700 and Mo_2C@2D-NPC/1100, Mo_2C@2D-NPC shows a smaller semicircle, suggesting that the catalyst carbonized at 900 ℃ has lower impedance, which is benefit for the HER performance.

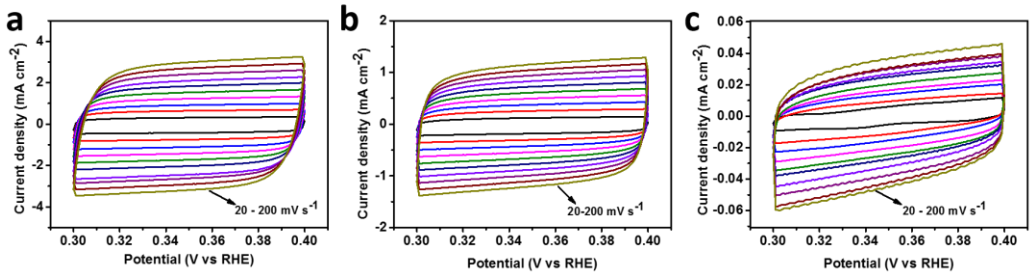

Figure S17. Cyclic voltammograms (CV) curves of (a) Mo_2C@2D-NPC, (b) Mo_2C@NPC, (c) com-Mo_2C with different rates from 20 to 200 mV s^{-1} in the region of 0.3 – 0.4 V *vs* RHE.

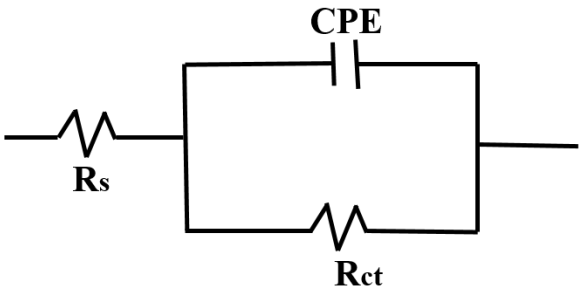

Figure S18. Equivalent circuit used for fitting of EIS data. R_s is the overall series resistance and R_{ct} is the charge transfer resistance, R_{ct} value generally varies inversely to the electrocatalytic activity. CPE is the constant phase angle element, which represents the double layer capacitance of solid electrode in the real-world situation.

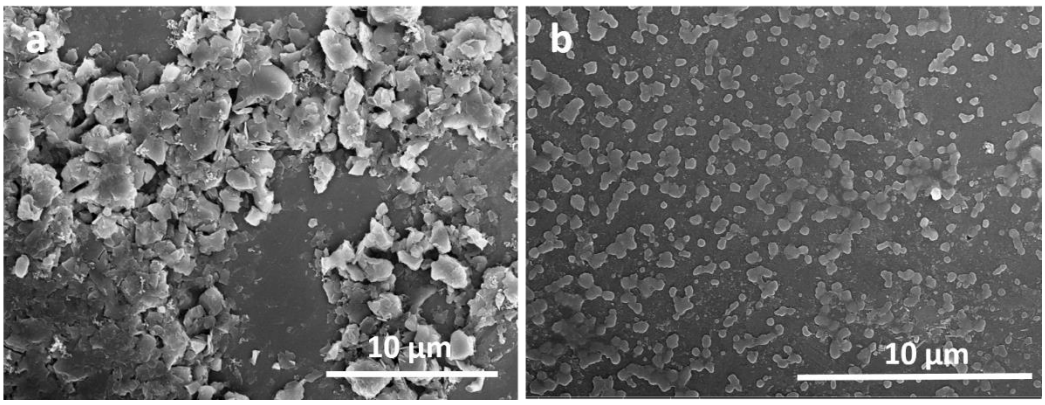

Figure S19. SEM image of com Mo_2C before and after ball-milled. (a) SEM image of original com Mo_2C, the com Mo_2C show the micro size; (b) SEM image of ball-milled com Mo_2C (bm-com Mo_2C), we obtained the submicron bm-com Mo_2C through the ball mill.

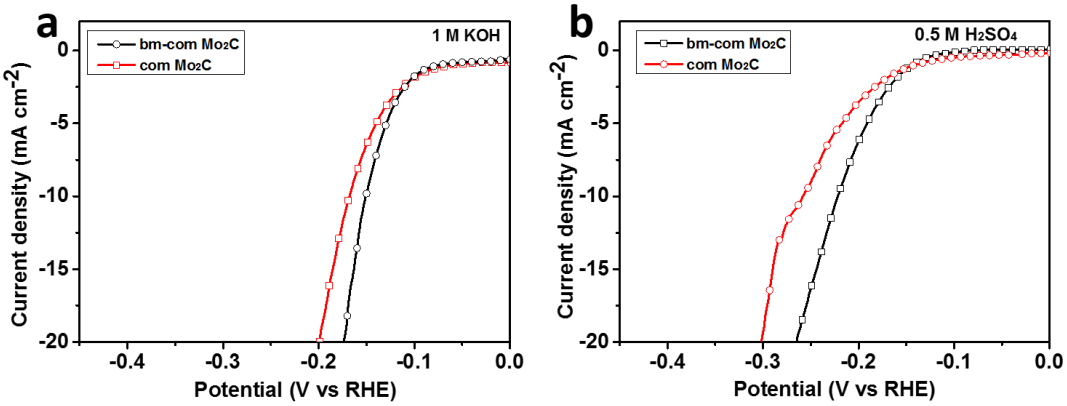

Figure S20. The performance contrast figure for the com Mo_2C and bm-com Mo_2C. (a) electrocatalysis HER performance of com Mo_2C and bm-com Mo_2C in 1 M KOH; (b) electrocatalysis HER performance of com Mo_2C and bm-com Mo_2C in 0.5 M H_2SO_4. It was found that no matter in alkaline or acid media, bm-com Mo_2C exhibited better performance. That's because after ball milling, the initial bulk particles were crushed into submicron size with larger proportion of exposed basal planes. Moreover, during the ball milling, catalytically active sites can be created because of crystalline defects and discontinuities, which were benefit for electrocatalysis, [1, 2] but still far beyond the state-of-the-art results (Table S4 and S5).

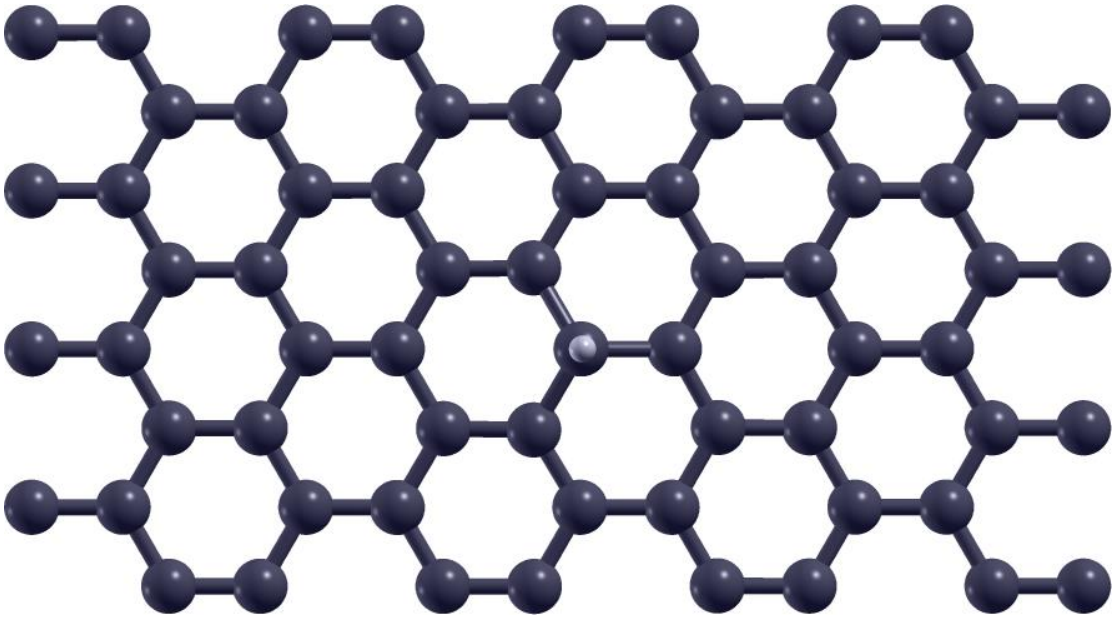

Figure S21. Hydrogen adsorbed on graphene (G) structure. A theoretical model description. The black and gray balls represent the C and H atoms.

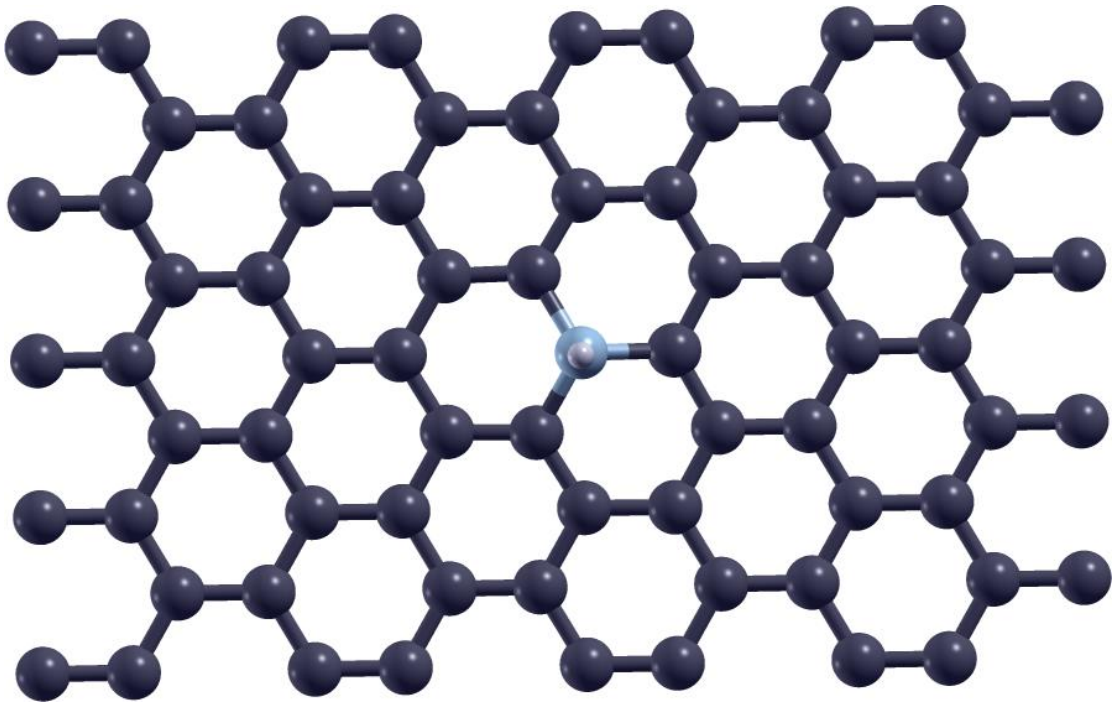

Figure S22. Hydrogen adsorbed on graphitic-N doped grapgene (GN). A theoretical model description. The black, gray and cyan balls represent the C, H and N atoms.

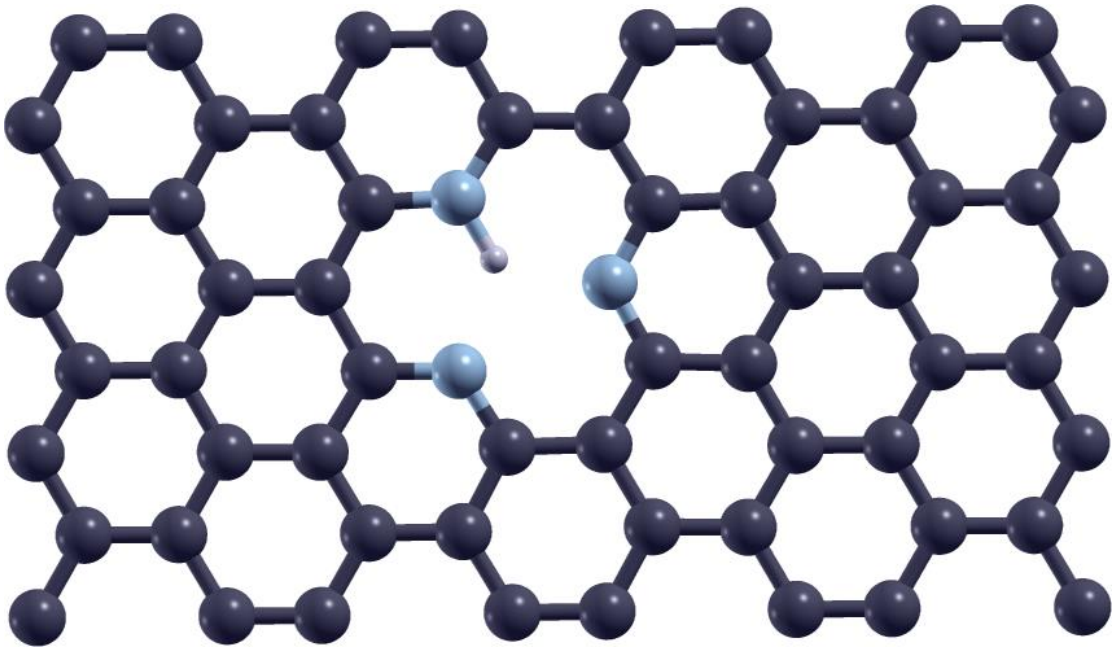

Figure S23. Hydrogen adsorbed on pyridinic-N doped graphene with one vacancy (Pyr.N3). A theoretical model description. The black, gray and cyan balls represent the C, H and N atoms.

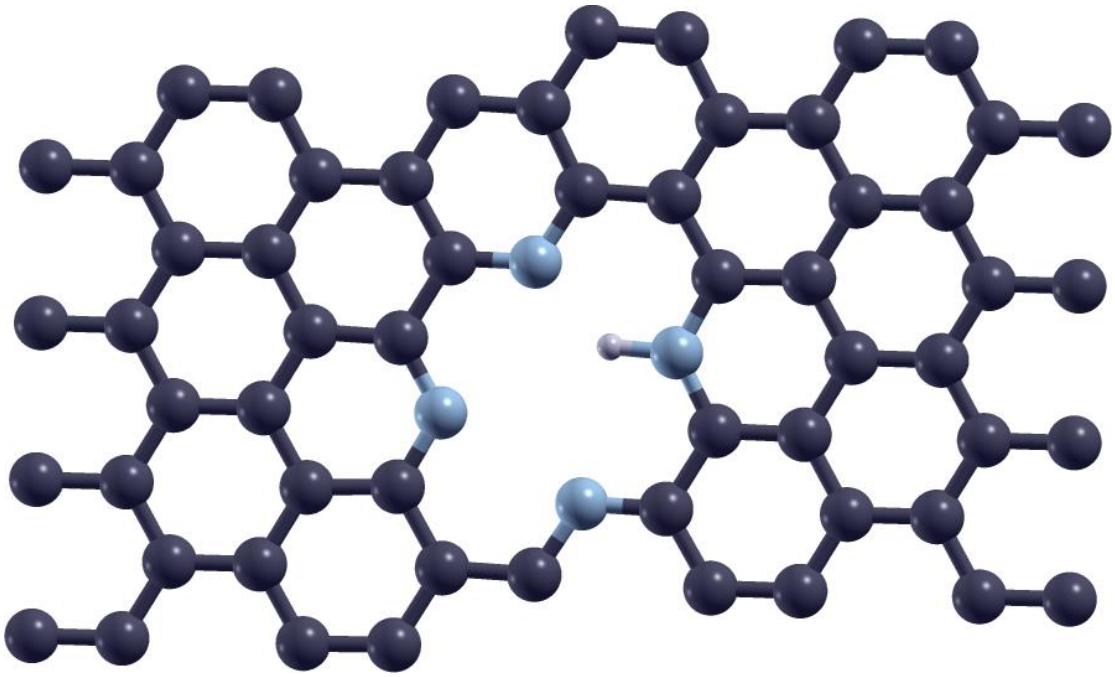

Figure S24. Hydrogen adsorbed on pyridinic-N doped graphene with two vacancies (Pyr.2VN3). A theoretical model description. The black, gray and cyan balls represent the C, H and N atoms.

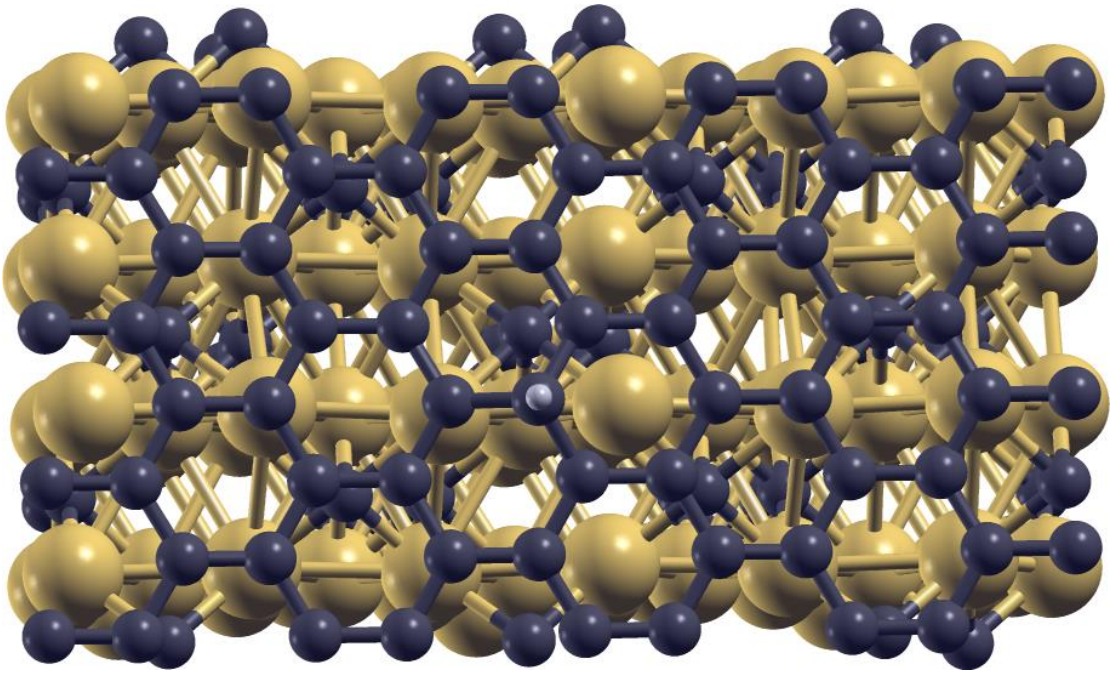

Figure S25. Hydrogen adsorbed on G@Mo_2C. A theoretical model description. The black, gray and brown balls represent the C, H and Mo atoms.

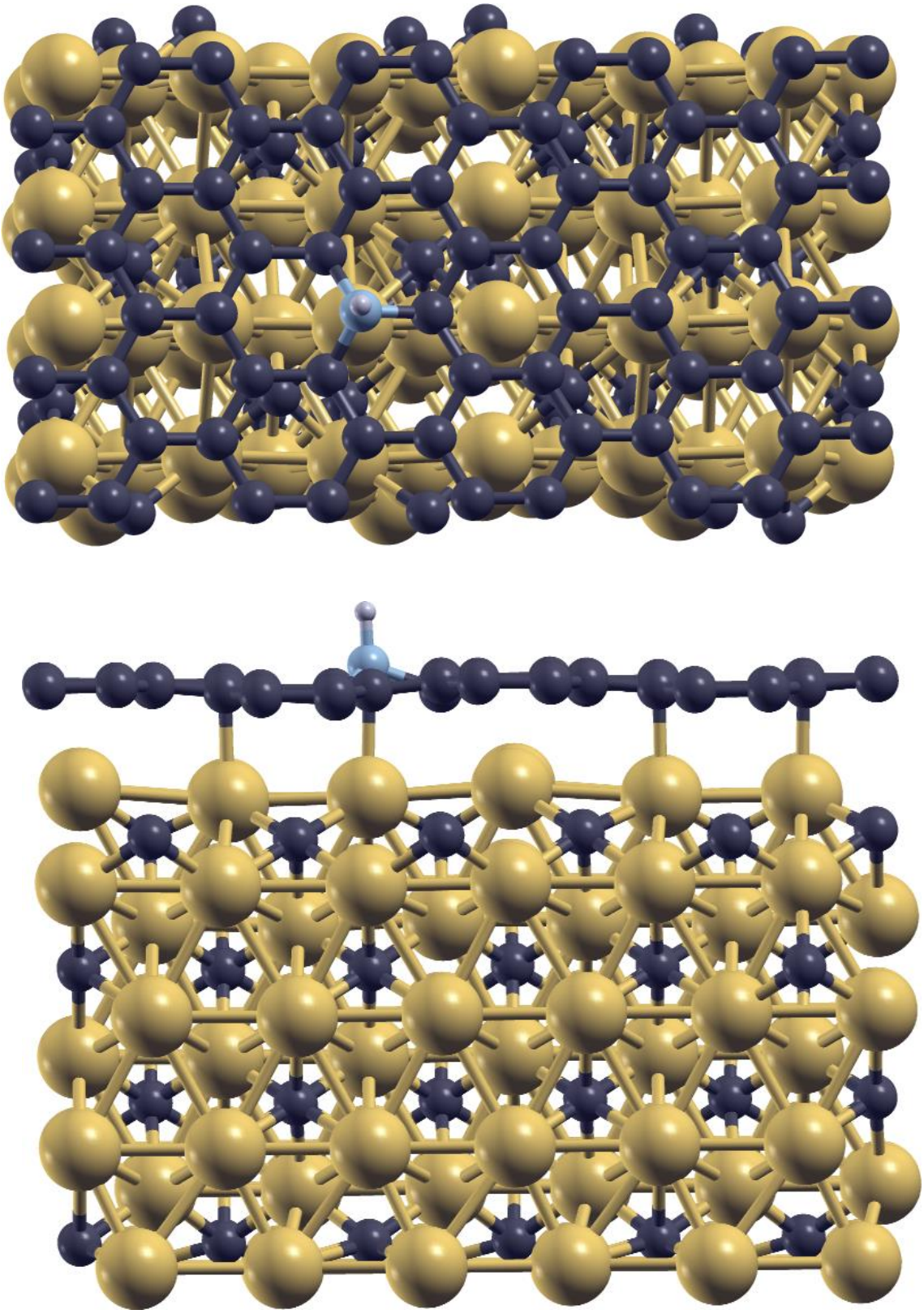

Figure S26. Hydrogen adsorbed on GN@Mo_2C. A theoretical model description. The black, gray, cyan, and brown balls represent the C, H, N and Mo atoms.

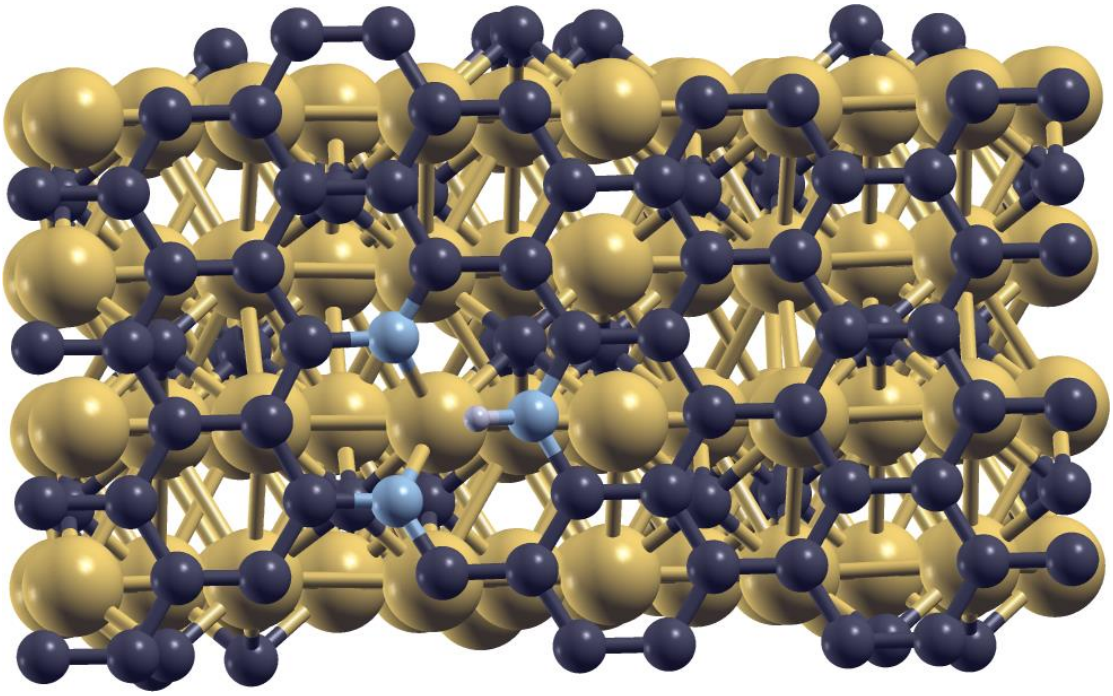

Figure S27. Hydrogen adsorbed on Pyr.N3@Mo_2C. A theoretical model description. The black, gray, cyan, and brown balls represent the C, H, N and Mo atoms.

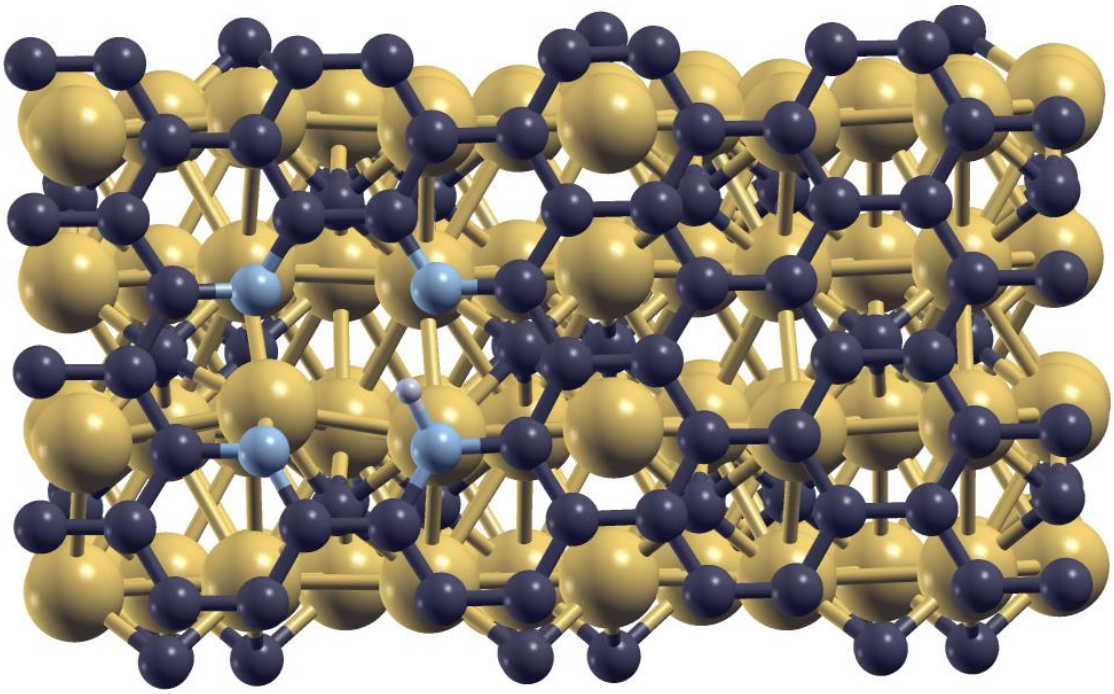

Figure S28. Hydrogen adsorbed on Pyr.2VN3@Mo_2C. A theoretical model description. The black, gray, cyan and brown balls represent the C, H, N and Mo atoms.

Table S1. N_2 sorption data for Mo_2C@2D-NPC, Mo_2C@NPC, and com-Mo_2C.

sample	S_{BET}/ (m^2 g^{-1}) [a]	$S_{langmuir}$/ (m^2 g^{-1}) [b]	V_{Tot}/ (cm^3 g^{-1}) [c]	D_{av}/ (nm) [d]
Mo_2C@2D-NPC	110.2	362.8	0.234	8.5
Mo_2C@NPC	72.7	194.3	0.193	10.6
com-Mo_2C	21.9	46.5	0.053	9.7

[a] Surface area (m^2 g^{-1}) calculated from the nitrogen adsorption based on the BET model. [b] Surface area (m^2 g^{-1}) calculated from the nitrogen adsorption isotherms based on the Langmuir model. [c] The total pore volume (cm^3 g^{-1}) calculated at P/P0 = 0.99. [d] Average pore diameter.

Table S2. Elemental analysis of C, Mo, N, and O based on XPS analysis

sample	C	Mo	N	O
	Element composition (at.%)			
Mo_2C@2D-NPC/700	60.21	7.90	19.26	12.63
Mo_2C@2D-NPC	65.79	6.31	15.62	12.28
Mo_2C@2D-NPC/1100	74.50	6.85	12.97	5.67
Mo_2C@NPC	72.00	3.25	8.68	16.07

Table S3. R_{ct} values of prepared Mo_2C-based samples.

sample	Rct
Mo_2C@2D-NPC	94
Mo_2C@NPC	1412
com-Mo_2C	18740
Mo_2C@2D-NPC/700	188
Mo_2C@2D-NPC/1100	231

From the above table, we can see that Mo_2C@2D-NPC shows the smallest value of Rct, which exhibits the fastest electron transfer properties among the samples.

Table S4. Comparison of HER performance in alkaline media for Mo_2C@2D-NPC with other electrocatalysts.

Catalyst	Current density (j, mA cm^{-2})	Overpotential at corresponding j (mV *vs* RHE)	Tafel slope (mV dec^{-1})	Reference
MoCx nano-octahedrons	10	151	59	3
Mo_2C@NC	10	60	/	4
Mo_2C nanotubes	10	112	55	5
MoP	10	130	48	6
CoP nanowire arrays	10	209	129	7
MoB	20	250	59	8
Ni_3S_2/nickel foam	10	223	/	9
Nanocrystalline Ni_5P_4	10	50	/	10
N,P/ Mo_2C@C	10	47	71	11
Mo_2C@NCF	10	100	65	12
Mo_2C@2D-NPC	**10** **20**	**45** **62**	**46**	**This work**

Table S5. Comparison of HER performance in acid media for Mo_2C@2D-NPC with other molybdenum carbide based electrocatalysts.

Catalyst	Current density (j, mA cm^{-2})	Overpotential at corresponding j (mV *vs* RHE)	Tafel slope (mV dec^{-1})	Reference
MoCx nano-octahedrons	10	142	53	3
Mo_2C@NC	10	124	60	4
Mo_2C nanotubes	10	172	62	5
N,P/ Mo_2C@C	10	141	58	11
Mo_2C@NCF	10	144	55	12
Mo_2C/CNT	10	152	65	13
Mo_2C nanowires	60	200	53	14
Co-Mo_2C	10	140	39	15
MoCN	10	140	46	16
Mo_2C@2D-NPC	**10** **20**	**86** **105**	**62**	**This work**

Reference:

(1) Wang, D.; Wang, Z.; Wang, C.; Zhou, P.; Wu, Z.; Liu, Z. Distorted MoS_2 Nanostructures: An Efficient Catalyst for the Electrochemical Hydrogen Evolution Reaction. *Electrochem. Commun.* **2013,** *34*, 219-222.

(2) Eckert, R.; Felderhoff, M.; Schüth, F. Preferential Carbon Monoxide Oxidation over Copper-Based Catalysts under *In situ* Ball Milling. *Angew. Chem., Int. Ed.* **2017,** *129*, 2485-2488.

(3) Wu, H. B.; Xia, B. Y.; Yu, L.; Yu, X.-Y.; Lou, X. W. D. Porous Molybdenum Carbide Nano-Octahedrons Synthesized *via* Confined Carburization in Metal-Organic Frameworks for Efficient Hydrogen Production. *Nat. Commun.* **2015,** *6*, 6512.

(4) Liu, Y.; Yu, G.; Li, G. D.; Sun, Y.; Asefa, T.; Chen, W.; Zou, X. Coupling Mo_2C with Nitrogen-Rich Nanocarbon Leads to Efficient Hydrogen-Evolution Electrocatalytic Sites. *Angew. Chem., Int. Ed.* **2015,** *54*, 10752-10757.

(5) Ma, F. X.; Wu, H. B.; Xia, B. Y.; Xu, C. Y.; Lou, X. W. D. Hierarchical β-Mo_2C Nanotubes Organized by Ultrathin Nanosheets as a Highly Efficient Electrocatalyst for Hydrogen Production. *Angew. Chem., Int. Ed.* **2015,** *54*, 15395-15399.

(6) Xiao, P.; Sk, M. A.; Thia, L.; Ge, X.; Lim, R. J.; Wang, J.-Y.; Lim, K. H.; Wang, X. Molybdenum Phosphide as an Efficient Electrocatalyst for the Hydrogen Evolution Reaction. *Energy Environ. Sci.* **2014,** *7*, 2624-2629.

(7) Tian, J.; Liu, Q.; Asiri, A. M.; Sun, X. Self-Supported Nanoporous Cobalt Phosphide Nanowire Arrays: an Efficient 3D Hydrogen-Evolving Cathode over the Wide Range of pH 0-14. *J. Am. Chem. Soc.* **2014,** *136*, 7587-7590.

(8) Vrubel, H.; Hu, X. Molybdenum Boride and Carbide Catalyze Hydrogen Evolution in Both Acidic and Basic Solutions. *Angew. Chem., Int. Ed.* **2012,** *124*, 12875-12878.

(9) Feng, L.-L.; Yu, G.; Wu, Y.; Li, G.-D.; Li, H.; Sun, Y.; Asefa, T.; Chen, W.; Zou, X. High-Index Faceted Ni_3S_2 Nanosheet Arrays as Highly Active and Ultrastable Electrocatalysts for Water Splitting. *J. Am. Chem. Soc.* **2015,** *137*, 14023-14026.

(10) Laursen, A.; Patraju, K.; Whitaker, M.; Retuerto, M.; Sarkar, T.; Yao, N.; Ramanujachary, K.; Greenblatt, M.; Dismukes, G. C. Nanocrystalline Ni_5P_4: a Hydrogen Evolution Electrocatalyst of Exceptional Efficiency in Both Alkaline and Acidic Media. *Energy Environ. Sci.* **2015,** *8*, 1027-1034.

(11) Chen, Y.-Y.; Zhang, Y.; Jiang, W.-J.; Zhang, X.; Dai, Z.; Wan, L.-J.; Hu, J.-S. Pomegranate-like N, P-Doped Mo_2C@C Nanospheres as Highly Active Electrocatalysts for Alkaline Hydrogen Evolution. *ACS Nano* **2016,** *10*, 8851-8860.

(12) Huang, Y.; Gong, Q.; Song, X.; Feng, K.; Nie, K.; Zhao, F.; Wang, Y.; Zeng, M.; Zhong, J.; Li, Y. Mo_2C Nanoparticles Dispersed on Hierarchical Carbon Microflowers for Efficient Electrocatalytic Hydrogen Evolution. *ACS Nano* **2016,** *10*, 11337-11343.

(13) Chen, W.-F.; Wang, C.-H.; Sasaki, K.; Marinkovic, N.; Xu, W.; Muckerman, J.; Zhu, Y.; Adzic, R. Highly Active and Durable Nanostructured Molybdenum Carbide Electrocatalysts for Hydrogen Production. *Energy Environ. Sci.* **2013,** *6*, 943-951.

(14) Liao, L.; Wang, S.; Xiao, J.; Bian, X.; Zhang, Y.; Scanlon, M. D.; Hu, X.; Tang, Y.; Liu, B.; Girault, H. H. A Nanoporous Molybdenum Carbide Nanowire as an Electrocatalyst for Hydrogen Evolution Reaction. *Energy Environ. Sci.* **2014,** *7*, 387-392.

(15) Lin, H.; Liu, N.; Shi, Z.; Guo, Y.; Tang, Y.; Gao, Q. Nanowires: Cobalt-Doping in Molybdenum-Carbide Nanowires Toward Efficient Electrocatalytic Hydrogen Evolution. *Adv. Funct. Mater.* **2016,** *26*, 5581-5581.

(16) Zhao, Y.; Kamiya, K.; Hashimoto, K.; Nakanishi, S. *In situ* CO_2-Emission Assisted Synthesis of Molybdenum Carbonitride Nanomaterial as Hydrogen Evolution Electrocatalyst. *J. Am. Chem. Soc.* **2014,** *137*, 110-113.